

## ■ Aggregation

## Understanding the Driving Mechanisms of Enhanced Luminescence Emission of Oligo(styryl)benzenes and Tri(styryl)-s-triazine

Rocío Domínguez,<sup>[b, c]</sup> Mónica Moral,<sup>[d]</sup> M. Paz Fernández-Liencres,<sup>[e]</sup> Tomás Peña-Ruiz,<sup>[e]</sup> Juan Tolosa,<sup>[b, c]</sup> Jesús Canales-Vázquez,<sup>[d]</sup> Joaquín C. García-Martínez,<sup>[b, c]</sup> Amparo Navarro,<sup>\*,[e]</sup> and Andrés Garzón-Ruiz<sup>\*,[a]</sup>

**Abstract:** This work is focused on unraveling the mechanisms responsible for the aggregation-induced enhanced emission and solid-state luminescence enhancement effects observed in star-shaped molecules based on 1,3,5-tris(styryl)-benzene and tri(styryl)-s-triazine cores. To achieve this, the photophysical properties of this set of molecules were analyzed in three states: free molecules, molecular aggregates in solution, and the solid state. Different spectroscopy and microscopy experiments and DFT calculations were conducted to scrutinize the causative mechanisms of the lumines-

cence enhancement phenomenon observed in some experimental conditions. Enhanced luminescence emission was interpreted in the context of short- and long-range excitonic coupling mechanisms and the restriction of intramolecular vibrations. Additionally, we found that the formation of  $\pi$ -stacking aggregates could block *E/Z* photoisomerization through torsional motions between phenylene rings in the excited state, and hence, enhancing the luminescence of the system.

## Introduction

The development of functional organic materials is a global aim for which self-assembly and the supramolecular architecture are critical factors that determine their applicability.<sup>[1,2]</sup> Consequently, control of the molecular self-assembly (dynamic or static) is currently a hot topic in different scientific disciplines, such as biology, chemistry, and materials science.<sup>[1–12]</sup> In-

trinsic characteristics of molecules, such as size, shape, and noncovalent forces, added to external factors, such as concentration, environmental polarity, viscosity, or temperature, govern the molecular arrangement of aggregates in the liquid phase.<sup>[2–6]</sup> In the solid state, these factors, linked to bulk material processing, determine the competition of multiple aggregation pathways for molecular building blocks (pathway complexity).<sup>[13]</sup> Leading the self-assembly of  $\pi$ -conjugated organic compounds is a challenging task that begins with the study of intrinsic and extrinsic factors that govern the molecular arrangement in the liquid phase, before bulk material processing. Effective control of molecular assembly has promising applications in different technological and scientific fields. For instance, some biomedical applications, such as biosensing, bioimaging,<sup>[14–19]</sup> and gene and drug delivery,<sup>[2,20,21]</sup> are based on molecular self-assembled systems. In addition, the crystal packing adopted by  $\pi$ -conjugated compounds determines their electronic and photophysical properties and their later use in light-emitting electronic devices,<sup>[1,14,15]</sup> chemiresistive sensors,<sup>[15,22]</sup> agricultural films,<sup>[23]</sup> among others.

Fluorescence spectroscopy is one of the most used techniques to study molecular self-assembly because fluorescence is very sensitive to changes in the molecular microenvironment, to restrictions of intramolecular motions, and to the electronic coupling between molecules.<sup>[24]</sup> Sometimes, the aim goes beyond investigating the type of aggregate and the target is control of the molecular self-assembly to improve the emissive properties of the material.<sup>[7,8,25–31]</sup> This is not a trivial issue because molecular aggregation generally leads to

[a] Prof. A. Garzón-Ruiz

Department of Physical Chemistry, Faculty of Pharmacy  
University of Castilla-La Mancha, José María Sánchez Ibañez s/n  
02071 Albacete (Spain)  
E-mail: andres.garzon@uclm.es

[b] Prof. R. Domínguez, Prof. J. Tolosa, Prof. J. C. García-Martínez

Department of Inorganic, Organic and Biochemistry  
Faculty of Pharmacy, University of Castilla-La Mancha  
José María Sánchez Ibañez s/n, 02071 Albacete (Spain)

[c] Prof. R. Domínguez, Prof. J. Tolosa, Prof. J. C. García-Martínez

Regional Center for Biomedical Research (CRIB)  
University of Castilla-La Mancha, Almansa s/n, 02071 Albacete (Spain)

[d] Prof. M. Moral, Prof. J. Canales-Vázquez

Renewable Energy Research Institute, University of Castilla-La Mancha  
Paseo de la Investigación 1, 02071 Albacete (Spain)

[e] Prof. M. P. Fernández-Liencres, Prof. T. Peña-Ruiz, Prof. A. Navarro

Department of Physical and Analytical Chemistry  
Faculty of Experimental Sciences, University of Jaén  
Campus Las Lagunillas, 23071, Jaén (Spain)  
E-mail: anavarro@ujaen.es Supporting information and the ORCID identification number(s) for the author(s) of this article can be found under:  
<https://doi.org/10.1002/chem.201905336>

quenching of the luminescence emission (aggregation-caused quenching (ACQ)). Fortunately, some compounds show enhanced luminescence upon aggregation (aggregation-induced enhanced emission (AIEE)), which increases their possible applications.<sup>[7,8,25–28]</sup> Different perspectives are used to explain this phenomenon: from conventional H or J aggregates, originating from Coulombic coupling in the framework of the theory of molecular excitons,<sup>[32–34]</sup> to the short-range excitonic coupling mechanism, due to wavefunction overlap between adjacent molecules.<sup>[35,36]</sup> On the other hand, the blocking of nonradiative relaxation by restriction of intramolecular vibrations (RIVs),<sup>[25,26]</sup> as well as restricted access to conical intersections (RACIs) between excited and ground states and the blocking of *Z/E* photoisomerizations are other mechanisms commonly used to interpret AIEE phenomena.<sup>[37,38]</sup>

Herein, we have studied the self-assembly processes in solution of a series of star- and cross-shaped molecules (Scheme 1) and their effect on the luminescence emission properties. In parallel, the aggregated supramolecular systems were modeled by means of DFT calculations to interpret the experimental observations and gain insights into why some of the studied molecules exhibited AIEE under certain experimental conditions. Herein, we have attempted to establish a relationship between the shape and chemical nature of the molecular core and differences observed in their photophysical behavior upon aggregation. Oligo(styryl)benzenes are interesting model molecules used in this study because they show strong luminescence emission in solution, tend to form  $\pi$ -stacking aggregates, and

have simple architectures and nearly symmetrical structures that allow rationalization of experimental results. Several investigations into the effect of aggregation on the photophysical properties of bis(styryl)benzene derivatives have been achieved,<sup>[38–42]</sup> but, unfortunately, the number of comparable studies published on tris(styryl)benzene and tetra(styryl)benzene is considerably reduced. We recently reported a study on the aggregation of molecule **1**, which is considered herein as a reference compound (although new experiments were also performed).<sup>[43]</sup> Molecules **2** and **3** will allow us to analyze the effect of the core size and the presence of nitrogen atoms in the molecular scaffold on the photophysical properties and the type of aggregate. Finally, the relationship between the luminescence emission properties and the supramolecular structure in the solid state was also investigated.

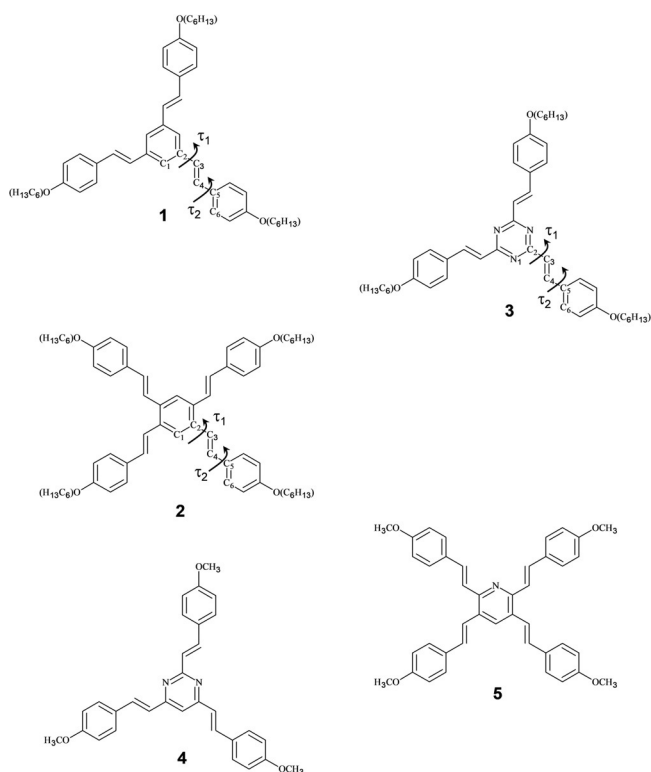
## Results and Discussion

### Synthesis

The syntheses of **1** and **2** are based on the Horner–Wadsworth–Emmons (HWE) reaction. This methodology has been extensively developed by us<sup>[44,45]</sup> and consists of the moisture-free reaction between phosphonates and aldehydes in the presence of potassium *tert*-butoxide, resulting in the styrylbenzene derivatives. Following this protocol, the isolation of **1** and **2** only requires the precipitation of the products in water after completion of the reaction. Compound **3** follows a similar reaction mechanism because the methyl groups of the triazine are acidic, but, in this case, NaOH (1 M) and Aliquat<sup>®</sup>, as a phase-transfer catalyst, were employed in a slight variation of an already reported procedure.<sup>[46]</sup> The *trans* stereochemistry of the double bonds was established on the basis of the coupling constant for the vinylic protons in the <sup>1</sup>H NMR spectra ( $J \approx 16$  Hz).

### Free molecules in solution

The spectroscopic behavior of the studied compounds was analyzed in the free-molecule state (in solution) before starting with aggregation experiments. Figure 1 shows the UV/Vis absorption and fluorescence emission spectra recorded for **1–3** in dichloromethane, and Table 1 collects the maximum absorption and emission wavelengths ( $\lambda_{ab}^{max}$  and  $\lambda_{em}^{max}$ , respectively) found in three different solvents (tetrahydrofuran, dichloromethane, and acetonitrile). No significant solvatochromic effects were observed in the absorption spectra and the lowest energy bands were assigned to  $\pi$ - $\pi^*$  transitions from the ground state to the  $S_1$  and  $S_2$  states (see Table S4 in the Supporting Information). In the case of the star-shaped molecules, the frontier molecular orbitals are not uniformly distributed on all branches of the conjugated core, leading to quasi-degenerate molecular orbitals and very close energies for transitions  $S_0 \rightarrow S_1$  and  $S_0 \rightarrow S_2$  (differences  $\leq 0.01$  eV, see Figure S11 in the Supporting Information). On the contrary,  $S_0 \rightarrow S_1$  and  $S_0 \rightarrow S_2$  transitions in compound **2** involve nondegenerate frontier orbitals, which are completely delocalized on the core; the differ-



**Scheme 1.** Structures of the studied compounds (**1–3**) showing the atom and bond numbering referred to in the molecular structure analysis. Structures of related compounds (**4** and **5**) mentioned herein are also included.

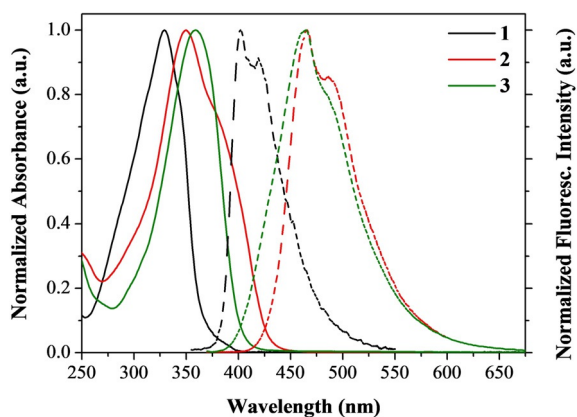


**Figure 1.** UV/Vis absorption and fluorescence emission spectra of compounds 1–3 in dichloromethane. The concentration of the samples was  $1 \mu\text{M}$  for the fluorescence emission spectra and  $5 \mu\text{M}$  for the UV/Vis absorption spectra.

**Table 1.** Maximum absorption wavelength ( $\lambda_{\text{ab}}^{\text{max}}$ ), molar absorption coefficient ( $\epsilon$ ), maximum emission wavelength ( $\lambda_{\text{em}}^{\text{max}}$ ), and fluorescence quantum yield ( $\Phi_{\text{F}}$ , concentration of the sample was  $1 \mu\text{M}$ ) determined for compounds 1–3 in various solvents (THF,  $\text{CH}_2\text{Cl}_2$  and  $\text{CH}_3\text{CN}$ ).

Compd. (solvent)	$\lambda_{\text{ab}}^{\text{max}}$ (eV [nm])	$\epsilon$ [ $\text{mM}^{-1} \text{cm}^{-1}$ ]	$\lambda_{\text{em}}^{\text{max}}$ (eV [nm])	$\Phi_{\text{F}}$ [%]
1 (THF) <sup>[a]</sup>	3.77 (329)	98.7	3.11 (399) 2.95 (420)	59.9
1 ( $\text{CH}_2\text{Cl}_2$ ) <sup>[a]</sup>	3.77 (329)	78.5	3.08 (403) 2.95 (421) (sh) <sup>[b]</sup>	40.0
1 ( $\text{CH}_3\text{CN}$ ) <sup>[a]</sup>	3.80 (326)	88.1	3.10 (400) 2.97 (417)	46.1
2 (THF)	3.54 (350)	97.2	2.69 (461)	56.7 <sup>[c]</sup>
2 ( $\text{CH}_2\text{Cl}_2$ )	3.54 (350)	85.6	2.66 (466)	43.3 <sup>[c]</sup>
2 ( $\text{CH}_3\text{CN}$ )	3.59 (345)	14.7	2.67 (465)	27.2 <sup>[c]</sup>
3 (THF)	3.48 (356)	59.5	2.82 (439)	0.1 <sup>[c]</sup>
3 ( $\text{CH}_2\text{Cl}_2$ )	3.45 (359)	92.6	2.67 (465)	0.4 <sup>[c]</sup>
3 ( $\text{CH}_3\text{CN}$ )	3.49 (355)	104.9	2.57 (482)	1.3 <sup>[c]</sup>

[a] From ref. [43]. [b] s h: shoulder. [c] Determined by using an integration sphere at room temperature. The concentration of the samples was  $1 \mu\text{M}$ . The excitation wavelength was 340 nm for 2 in THF and  $\text{CH}_2\text{Cl}_2$ , 335 nm for 2 in  $\text{CH}_3\text{CN}$ , 350 nm for 3 in THF, and 345 nm for 3 in  $\text{CH}_2\text{Cl}_2$  and  $\text{CH}_3\text{CN}$ . Excitation and emission slits were 10.0 and 0.25–0.28 nm, respectively. Dwell time was 0.5 s.

ence in energy between both transitions (0.34 eV, in dichloromethane) is significantly higher than that in the case of 1 and 3 (see Table S4 in the Supporting Information). As discussed below, the redshift observed for 2 with respect to 1 could be related to its more extended and more effective conjugation.<sup>[47]</sup> It must also be noted that the fluorescence maximum wavelength is only sensitive to the polarity of the solvent for compound 3 (the emission energy decreases as the polarity of the solvent increases; see Table 1). This fact can be associated with intramolecular charge-transfer processes from the styryl branches, where HOMO is mainly localized, to the *s*-triazine ring, which has a high contribution to the LUMO.<sup>[48]</sup> The chosen method (TD-M06-2X/6-31G\*) showed a reasonable performance in the calculations of electronic vertical transition energies for the studied compounds, particularly for compounds

without nitrogen atoms in the core. Thus, considering the solutions in dichloromethane as a reference, the differences found between the energy calculated for the lowest lying absorption transition and the corresponding experimental value are  $\leq 0.26$  eV for compounds 1 and 2. Similar energy differences were observed between the experimental and calculated fluorescence emission maxima of these compounds ( $\leq 0.26$  eV). On the contrary, the divergence between calculated and experimental emission maxima reached 0.45 eV in the case of compound 3.

As discussed in the following section, the extension and shape of the  $\pi$ -conjugated system, as well as the planarity of the core, are key parameters that control the self-assembly processes and, therefore, must be thoroughly analyzed herein. In addition, conformational changes produced in the core during electron excitation will play a critical role in the photo-physical properties, not only in the free-molecule state, but also in molecular aggregates. Thus, although the  $\pi$ -conjugated core of 2 is less planar than that of the cores of the star-shaped molecules (the main differences are associated with the value of the dihedral angle,  $\tau_1$ , between the central ring and the vinylene groups; see Scheme 1, Figure 2, and Figure S12 and Table S3 in the Supporting Information), the conjugation in this molecule is more extended and seems to be more effective. As already discussed in our previous study,<sup>[47]</sup> a comparative analysis of the C–C stretching modes in the high-energy region of the Raman spectra is a reliable indicator of  $\pi$

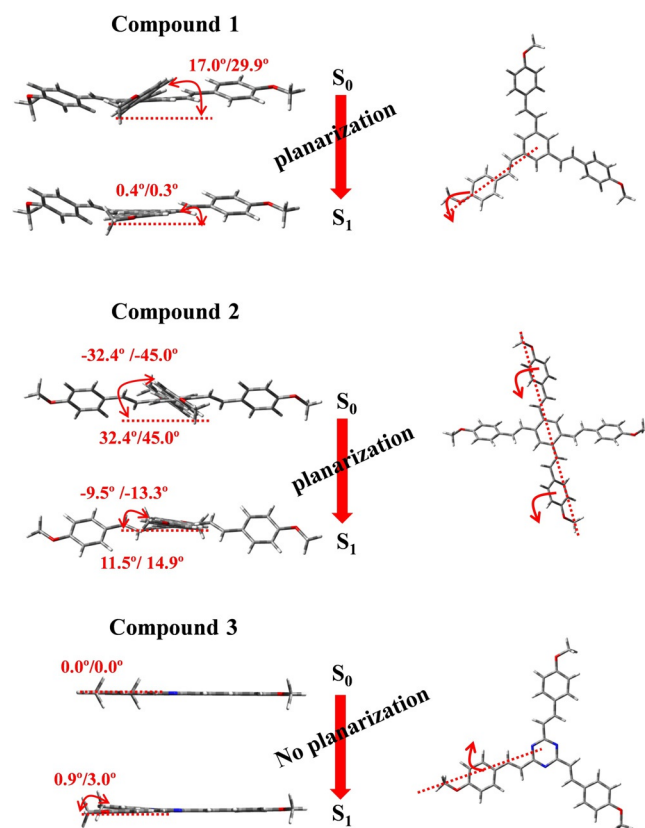


**Figure 2.** Schematic representation of the geometry changes for the  $\tau_1$  and  $\tau_2$  dihedral angles in compounds 1, 2, and 3 after photoexcitation ( $S_0 \rightarrow S_1$ ) calculated at the M06-2X/6-31G\* level of theory in dichloromethane.

conjugation. Thus, the C–C stretching of the vinylene groups appears in **2** at lower energy than that in **1**; the observed (calculated) values are 1624 (1650) and 1633  $\text{cm}^{-1}$  (1658  $\text{cm}^{-1}$ ), respectively, which suggest more effective  $\pi$  conjugation in **2** with respect to its counterpart, **1** (see Figures S4 and S5 in the Supporting Information).

On the other hand, the most planar core was predicted for compound **3**, with dihedral angles  $\tau_1$  and  $\tau_2$  close to zero (see Figure 2 and Figure S12 and Table S3 in the Supporting Information). This high planarity could be related to intramolecular interactions established between the nitrogen atoms of the *s*-triazine ring and the closest hydrogen atoms of the vinylene groups are the computed N...H distances (2.45–2.46 Å) smaller than the sum of their van der Waals radii (see Figure S13 in the Supporting Information).<sup>[49]</sup> The low fluorescence quantum yields ( $\Phi_F < 2\%$ ) found for compound **3** contrast with the high oscillator strengths,  $f$ , calculated for its lowest energy vertical transitions (comparable to those obtained for **1**; see Table S4 in the Supporting Information). Here, it should also be remembered that the Strickler–Berg relation establishes that the radiative rate constant ( $k_r$ ) is directly related to  $f$ .<sup>[50,51]</sup> Therefore, the presence of nitrogen atoms in the core leads to a luminescence deactivation, as already reported in a previous study on the photophysical properties of carbazolyl derivatives of **1** and **3**.<sup>[48]</sup> In this sense, a fluorescence quantum yield in dichloromethane of 15% was reported for a star-shaped molecule analogous to **1** and **3**, but with a pyrimidine central ring (compound **4**).<sup>[52]</sup> This value is higher than that of the quantum yield measured for the *s*-triazine derivative (compound **3**;  $\Phi_F = 0.4\%$ ), but significantly lower than that reported for the tri-branched molecule without nitrogen atoms (compound **1**;  $\Phi_F = 40.0\%$ ) in the same solvent.<sup>[43]</sup> Similarly, a fluorescence quantum yield in dichloromethane of 33% was reported for compound **5**, a cross-shaped molecule with a pyridine central ring, whereas the  $\Phi_F$  value measured here for an analogous molecule without nitrogen atoms in the core (compound **2**) amounts to 43.3%.<sup>[53]</sup> Different mechanisms could contribute to the nonradiative deactivation of compound **3**, such as intramolecular charge-transfer quenching,<sup>[54–56]</sup> intramolecular motions that lead to a deformation of the molecular structure in the excited state,<sup>[57]</sup> and *E/Z* photoisomerizations.<sup>[38,53,58,59]</sup> DFT calculations showed that the planarity of the molecular structure of **3** was slightly reduced in the  $S_0 \rightarrow S_1$  excitation process, in contrast with the planarization observed for **1** and **2** upon excitation (one or two styryl branches are significantly planarized in the case of compounds **1** and **2**, respectively, through the dihedral angles  $\tau_1$  and  $\tau_2$ ). Figure 2 provides a schematic representation of the most dramatic changes predicted in the molecular geometry upon excitation. Accordingly, the vibronic structure of the fluorescence emission spectra is more clearly observed for compounds **1** and **2** in all solvents used (see Figures 1 and 3 and Figure S8 in the Supporting Information); this suggests that these compounds adopt a more planar and conjugated structure in the excited state than that of **3**.<sup>[24]</sup> The shortest average fluorescence lifetime ( $\tau_{av}$ ) was obtained for compound **3**, showing that the nonradiative deactivation pathways are more efficient for this compound than those for **1**

and **2** ( $\tau_{av} = 8.18, 6.11,$  and  $0.19$  ns for **1**, **2**, and **3**, respectively, in THF at 298 K). Nevertheless,  $\tau_{av}$  is significantly more sensitive to the temperature in the case of **3**, increasing by two times from 298 to 268 K (see Table S1 in the Supporting Information). The molecular movements are more restricted at low temperature, increasing the fluorescence lifetime due to the reduction of the nonradiative rate constant ( $k_{nr}$ ).

## Aggregation studies in solution

### The 1,3,5-tris(styryl)benzene core

AIEE was already observed for compound **1** in mixtures of water/acetonitrile with water fractions ( $f_w$ ) of  $\leq 40\%$  in our previous study.<sup>[43]</sup> Here, we have found that this compound also exhibits AIEE in mixtures of water/THF, reaching a maximum quantum yield for  $f_w = 50\%$  ( $\Phi_F = 65\%$ ; see Figures 3 and 4). Despite the fluorescence intensity enhancement, only small band shifts were observed for these samples in both the absorption and emission spectra. In the framework of the theory of molecular excitons, this behavior could be associated with aggregation of orthogonal transition dipole moments of the molecular units in which the electronic coupling is generally weak.<sup>[60,61]</sup> Accordingly, only small spectral shifts ( $\leq 0.03$  eV)<sup>[43]</sup> and weak electronic couplings ( $< 71$  meV) for both holes ( $t_h$ ) and electrons ( $t_e$ ) have been computed for the most energetically stable molecular aggregate of **1** in aqueous solution (see Table 2 and Figure S19 in the Supporting Information). Here, it must be remembered that the product,  $|t_h t_e|$ , gives an idea about the short-range charge-transfer interactions in the context of the theory reported by Spano and Hestand.<sup>[35,36]</sup> The AIEE effect based on the so-called X aggregates has been reported for different  $\pi$ -conjugated systems.<sup>[61–64]</sup> In the case of weak electronic couplings, the phenomenon of AIEE could be related to different effects, such as the reduction of oxygen quenching and the formation of a hydrophobic microenvironment inside the aggregate, as well as the blocking of photochemical processes such as *E/Z* isomerization in the excited singlet state.<sup>[38,65]</sup> It is well known that styryl-substituted benzenes undergo *E/Z* photoisomerizations; the *Z,E,E*-conformer of 1,3,5-tris(styryl)benzene is less fluorescent than that of the *E,E,E*-conformer.<sup>[38,53,58,59]</sup> The lower temperature and increase in the viscosity of the medium hinder this type of deactivation process associated with changes in the molecular geometry, and thus, increase the value of the fluorescence quantum yield and lifetime.<sup>[58,59]</sup> Accordingly, the formation of stacking aggregates should block the *E/Z*-photoisomerization processes and increase the luminescence emission. Based on our calculations, the RIV mechanism could also contribute to luminescence enhancement in the aggregated state of **1**. Three significant Huang–Rhys (HF) factors values ( $> 1.5$ ) involved in the nonradiative internal conversion decay have been predicted for this compound in aqueous solution (see Figure 5 and Figure S14 in the Supporting Information for additional information in both aqueous solution and dichloromethane). These HF factor values are associated with low vibrational frequencies of 15, 22, and 25  $\text{cm}^{-1}$ ; this implies a wide wagging of the molecule as a whole, which could be blocked by stacking aggregation

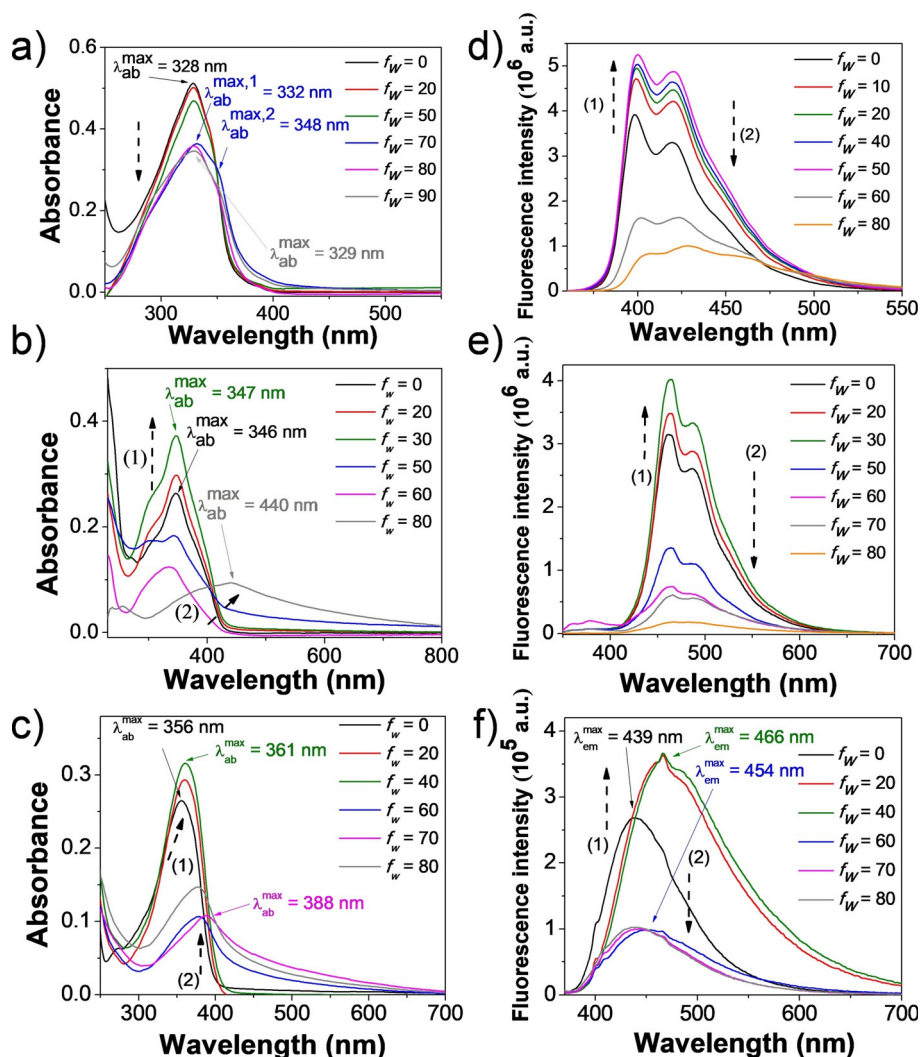


**Figure 3.** Absorption and fluorescence emission spectra of compounds 1 (a,d), 2 (b,e), and 3 (c,f) in mixtures of H<sub>2</sub>O/THF at different water fractions ( $f_w$ ; the concentration of the samples was 5  $\mu$ M; temperature was kept at 298 K). Some spectra have been removed for simplicity.

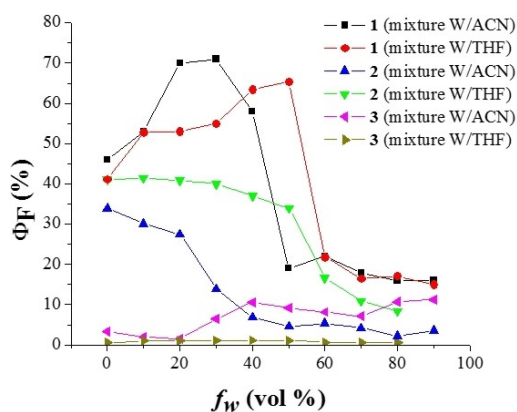


**Figure 4.** Fluorescence quantum yield ( $\Phi_F$ ) measured in mixtures of water (W)/CH<sub>3</sub>CN and W/THF for compounds 1, 2, and 3;  $f_w$  is the water fraction in volume percentage. The concentration of the samples was 5  $\mu$ M. The excitation wavelength was 330 nm; the excitation and emission slits were 10 and 0.25–0.36 nm, respectively; and the dwell time was 0.2 s. Data corresponding to compound 1 in mixtures of W/CH<sub>3</sub>CN were reported in ref. [43].

**Table 2.** Hole and electron coupling ( $t_h$  and  $t_e$ , respectively) calculated for dimers extracted from the most energetically stable molecular clusters (containing four stacked molecules) optimized for the compounds studied.  $d_{cc}$  is the distance between centroids of the central benzene/triazine rings of neighboring molecules.  $d_{pp}$  corresponds to the distance between parallel planes containing the central benzene/triazine rings of neighboring molecules. All of these parameters were calculated for the central dimer of each tetramer.

Compd.	Species (medium) <sup>[a]</sup>	$ t_e $ [meV]	$ t_h $ [meV]	$ t_h t_e $ [meV]	$d_{cc}$ [Å]	$d_{pp}$ [Å]
1 <sup>[b]</sup>	t <sub>1</sub> (gas phase)	10.7	7.3	79	3.54	3.54
1 <sup>[b]</sup>	t <sub>2</sub> (aq. sol.)	48.7	70.8	3446	4.12	3.16
2	t <sub>1</sub> (gas phase)	5.4	11.6	63	3.62	3.43
2	t <sub>1</sub> (aq. sol.)	17.1	11.4	196	3.62	3.43
3	t <sub>1</sub> (gas phase)	41.2	20.4	841	3.55	3.13
3	t <sub>1</sub> (aq. sol.)	34.2	25.3	864	3.53	3.14

[a] Aq. sol. is aqueous solution. [b] Tetramer clusters were calculated in a previous study.<sup>[43]</sup>

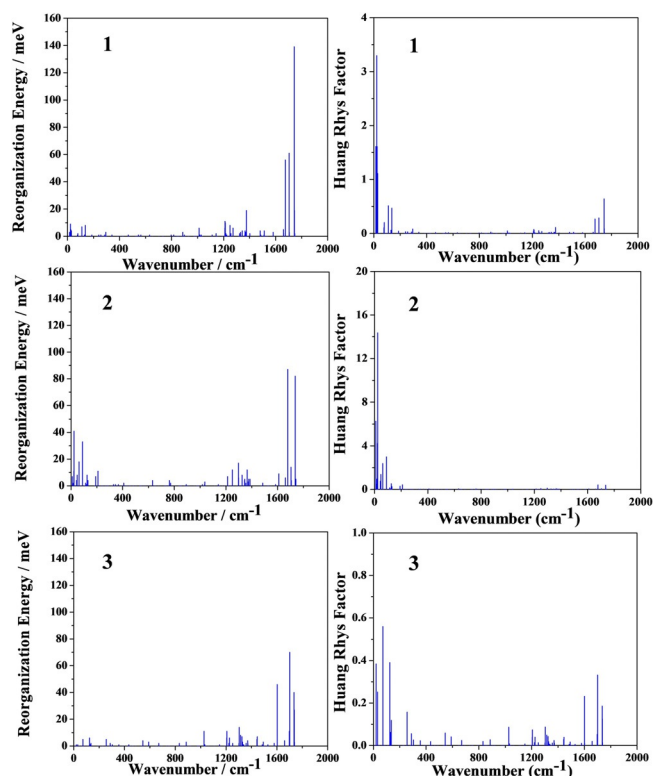


**Figure 5.** Reorganization energy (in eV) and HR factor versus normal-mode wavenumber (in  $\text{cm}^{-1}$ ) for compounds 1, 2, and 3 in the ground state calculated in aqueous solution at the M06-2X/6-31G\* level of theory.

(see Figure S15 in the Supporting Information).<sup>[66]</sup> Both RIVs and the blocking of *E/Z* photoisomerization upon aggregation are mechanisms consistent with the increase of the fluorescence lifetime reported for compound 1 upon going from  $f_w = 0$  to 30% in mixtures of water/acetonitrile due to a reduction of the nonradiative rate constant.

The increase of  $f_w$  above 50%, in both solvent mixtures, induces a luminescence decrease and small bathochromic shifts. The product  $|t_h t_e|$  increases from 0.08 eV, for the most energetically stable molecular aggregate in the gas phase (tetramer  $t_1$ ), to 3.45 eV, for the most stable aggregate in aqueous solution (tetramer  $t_2$ ; see Table 2 and Figure S19 in the Supporting Information).<sup>[43]</sup> Hence, an increase of the polarity of the medium could lead to a decrease in the  $\pi$ -stacking distance and sliding of the monomeric subunits in the aggregate, and thus, increasing the electronic coupling. Thus, the luminescence could be quenched because of stronger coupling between monomeric subunits. In addition, sliding between neighboring molecules should partially relax the restriction of the normal modes involved in the nonradiative internal conversion decay (low frequencies associated with the wide molecular wagging previously described). Both phenomena would explain well the decrease in the fluorescence lifetimes in mixtures of water/acetonitrile with  $f_w = 50$  and 80%, in parallel to the drop of the fluorescence quantum yield (see Figure 4 and Table 3).

**Table 3.** Steady-state fluorescence anisotropy ( $r$ ) and average fluorescence lifetime ( $\tau_{av}$ ) of compounds 1–3 in different mixtures of water and acetonitrile. Lifetimes were measured at different emission wavelengths.<sup>[a]</sup>

Compd.	$f_w$ [%]	$r$	$\tau_{av}$ [ns]			
			$\lambda_{em} = 400$ nm	$\lambda_{em} = 450$ nm	$\lambda_{em} = 500$ nm	$\lambda_{em} = 550$ nm
1 <sup>[b]</sup>	0	0.022	8.09	–	7.93	–
	30	0.044	9.69	–	10.11	–
	50	0.147	6.68	–	6.99	–
	80	0.217	3.71	–	5.65	–
2 <sup>[c]</sup>	0	0.044	–	5.50	–	5.63
	20	0.038	–	5.31	–	4.50
	40	0.052	–	3.30	–	3.51
	70	0.084	–	0.92	–	3.63
3 <sup>[d]</sup>	0	0.070	–	0.59	–	0.76
	30	0.144	–	0.89	–	3.07
	60	0.294	–	1.49	–	5.81

[a] The concentration of the samples was 5  $\mu\text{M}$  and the temperature was kept at 25 °C. [b] From reference [43]. [c] Steady-state anisotropy was measured at  $\lambda_{em} = 461$  nm. The samples were excited at  $\lambda = 368$  nm to record the fluorescence decays. [d] Steady-state anisotropy was measured at  $\lambda_{em} = 482$  nm. The samples were excited at  $\lambda = 368$  nm to record the fluorescence decays.

### The 1,2,4,5-tetra(styryl)benzene core

Two different scenarios were also observed regarding the photophysical properties of the aggregates of compound 2, depending on the polarity of medium, that is, in solvent mixtures with low and high water fractions. At low water fractions, the fluorescence quantum yield of compound 2 remains near the value measured for  $f_w = 0$  and subsequently drops for mixtures of water/acetonitrile of  $f_w \geq 30\%$  and mixtures of water/tetrahydrofuran of  $f_w \geq 60\%$  (see Figure 4). Hence, no AIEE phenomenon was found for compound 2 in solution, in contrast with 1. It must be noted that the conversion from emissive aggregates to weakly emissive aggregates occurs at lower water fractions in mixtures of water/acetonitrile (more polar) than that in mixtures of water/tetrahydrofuran (less polar) for both compounds 1 and 2. This reveals the influence of the polarity of the medium on the control of the type of aggregate. Insignificant spectral shifts were observed in mixtures of water/tetrahydrofuran at low water fractions, whereas a blueshifted band and a broad redshifted band appeared at  $f_w \geq 10$  and 30%, respectively, in mixtures of water/acetonitrile (see Figure 4 and Figures S7 and S8 in the Supporting Information).

DFT calculations and additional spectroscopic experiments were conducted to unravel the differences observed in the photophysical behavior of compound 2 with respect to that of 1. A cluster composed by four stacked molecules of 2 was optimized by employing the fully overlapped configuration as a starting point. This configuration is the most energetically favored arrangement obtained from the azimuthal barrier and binding-energy landscape that were previously carried out for a stacked dimer (see Figure 6). In this molecular cluster, the monomeric units of 2 are weakly coupled, in comparison with those in 1 and 3, which could reduce the fluorescence quenching efficiency in the molecular aggregate (see Table 2). In addition, we hypothesize that RIV is a less efficient mechanism,

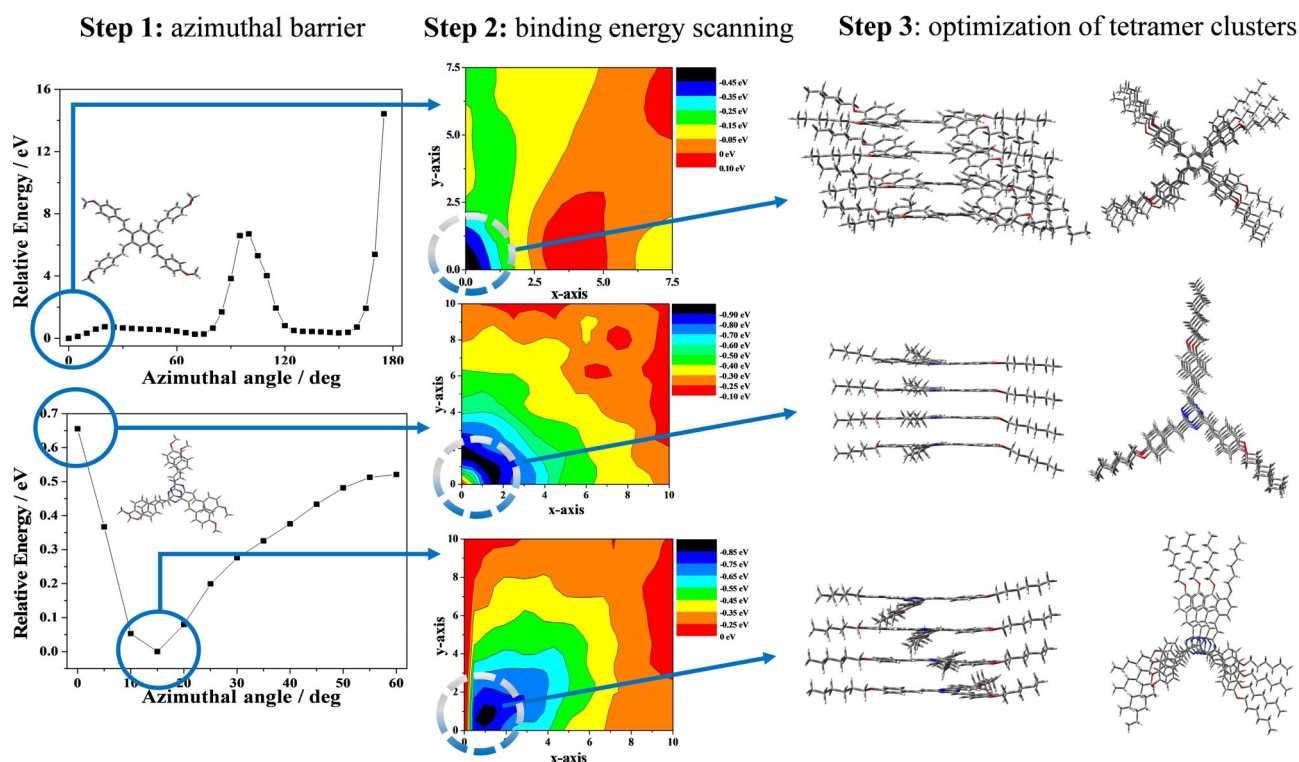


**Figure 6.** Steps in the optimization of tetramer clusters for compounds **2** and **3**. Step 1: azimuthal barrier. The relative energy versus azimuthal angle ( $\varphi$ ) calculated at the M06-2X/6-31G\* level of theory is shown (see also Figure 9; the intermolecular distance was fixed at 5.1 Å for **2** and 3.5 Å for **3**). Step 2: binding-energy landscape in the  $x,y$  plane calculated at the M06-2X/6-31G\* level of theory (see Figure 9). The binding-energy landscapes were carried out for molecule **2** with  $\varphi=0^\circ$  and for molecule **3** with  $\varphi=0$  and  $15^\circ$ . Step 3: optimized structure of tetramer clusters in aqueous solution at the M06-2X/6-31G\*/M06-2X/STO-3G level of theory obtained by employing the molecular arrangement of the maximum binding energy obtained in step 2 as the starting point.

during electronic relaxation, in the aggregates of compound **2** than in those formed by **1** because up to seven normal modes with significant HR factor values (from 1.4 to 14.4) are found, and some of them correspond to slight rocking of the phenyl rings (for instance,  $\omega=61\text{ cm}^{-1}$  with HR=2.4 and  $\omega=89\text{ cm}^{-1}$  with HR=3.0; see Figure S16 in the Supporting Information). These molecular vibrations cannot be completely blocked in a  $\pi$ -stacking aggregate and keep contributing to the nonradiative deactivation. Regarding  $E/Z$  photoisomerization, Oelkrug et al. reported that this process in stilbenes depended on steric effects, as well as on the temperature and viscosity of the medium.<sup>[58]</sup> Therefore,  $E/Z$  isomerization in the excited state could not be an efficient nonradiative deactivation mechanism in molecule **2** because this is more sterically congested than that in **1**. In this sense, the torsional barrier around the vinylene moiety (dihedral angle  $\alpha$ ) was calculated for all studied compounds in the  $S_1$  excited state to deepen our understanding of its role in  $E/Z$  photoisomerization as a nonradiative deactivation process (see Figure 7). Obtaining a complete description of the potential energy surface of the  $S_1$  state of these compounds is out of the scope of the current study and could become extremely complex and prohibitively demanding (see ref. [67] and references therein). Nevertheless, in the scanned region (from  $\alpha=0$  to  $45^\circ$ ), it was found that the energy required for this rotation was significantly higher for compound **2** than that for **1**, according to the lower efficiency expected for  $E/Z$  photoisomerization of the tetrabranched molecule as a

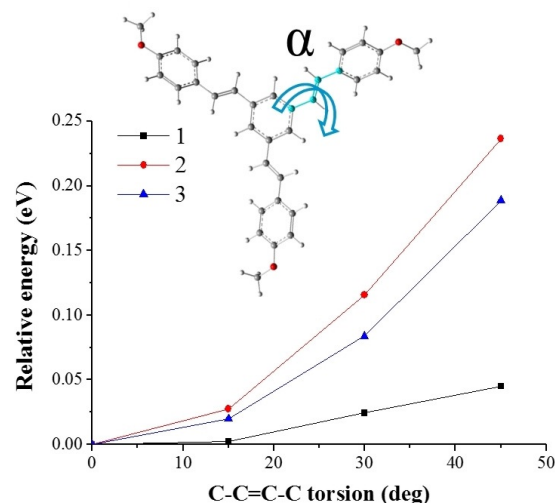


**Figure 7.** Torsional barriers around the vinylene moiety in the  $S_1$  excited state of compounds **1–3**. The zero level of energy corresponds to the *all-trans* configuration.

nonradiative deactivation mechanism. Hence, in weakly coupled aggregates (at low water fractions),  $k_{nr}$  could not be substantially reduced by RIV and blocking of the  $E/Z$  photoisomerization and, consequently, AIEE was not observed for compound **2**, in contrast to that of **1**.

As shown in Figure 3 and Figures S7 and S8 in the Supporting Information, significant spectral changes were observed for high water fractions, which suggested that the molecules in the aggregate were more strongly coupled under these experimental conditions than those in previously discussed experiments (see, for instance, the redshifted band centered at  $\lambda = 440$  nm that appears in mixture of water/tetrahydrofuran at  $f_w = 80\%$ ). Theoretical calculations predicted the existence of a weak redshifted transition ( $S_0 \rightarrow S_2$ , with a low oscillator strength,  $f = 0.12$ , and  $\Delta E = -0.06$  eV) and a strong blueshifted band involving two closed transitions with high oscillator strengths ( $S_0 \rightarrow S_6$ ,  $f = 3.60$ ,  $\Delta E = 0.19$  eV;  $S_0 \rightarrow S_7$ ,  $f = 0.99$ ,  $\Delta E = 0.22$  eV) for the tetramer cluster previously optimized in aqueous solution ( $\Delta E$  is the difference in energy between those vertical transitions and the lowest energy transition calculated for a single molecule under the same conditions; see Table S5 in the Supporting Information for more details). Fluorescence anisotropy increased with the water fraction, which suggested that the movement of the molecule was more restricted in aggregates formed at high water fractions than that in aggregates observed at low water fractions (see Table 3). In this sense, the product  $|t_h t_e|$  calculated for the molecular aggregates in aqueous solution is about threefold with respect to the gas phase; this also indicates that the electronic coupling strength increases in polar media. Under these experimental conditions, compound **2** shows similar behavior to that of **1**, that is, luminescence seems to be quenched due to stronger coupling between monomeric subunits. The fluorescence lifetime keeps decreasing upon the addition of water, but, at high water fractions, a significant difference found for  $\tau_{av}$  measured at different wavelengths suggests the coexistence of different emissive species (0.92 ns at  $\lambda = 450$  nm and 3.63 ns at  $\lambda = 550$  nm, for mixtures of water/acetonitrile with  $f_w = 70\%$ ; see Table 3).

### The tri(styryl)-s-triazine core

The *s*-triazine derivative showed distinct photophysical behavior not previously observed for compounds **1** and **2**. In pure solvents, the lowest fluorescence quantum yields were determined for compound **3** and, in solvent mixtures, its quantum yield remained near the value measured for  $f_w = 0$  ( $\Phi_F \leq 3\%$ ). Contrary to compounds **1** and **2**, the AIEE phenomenon was found at high water fractions of mixture of water/acetonitrile, reaching a fluorescence quantum yield of 11%. New redshifted bands associated with the formation of molecular aggregates appeared in the absorption spectrum at high water fractions in mixtures of both water/acetonitrile and water/tetrahydrofuran (see Figure 3 and Figure S7 in the Supporting Information).

For this molecule, two clusters composed of four stacked molecules were optimized by following a procedure previously described (as illustrated in Figure 6), that is, the binding energy was scanned for stacked dimers with  $\varphi = 0$  and  $15^\circ$  ( $\varphi = 15^\circ$  is the energy minimum of the azimuthal barrier); two tetramer clusters ( $t_1$  and  $t_2$ ) were optimized by using the most energetically favorable arrangement of each binding-energy landscape as a starting point. In both the gas phase and aqueous

solution,  $t_1$  (obtained from the binding-energy landscape with  $\varphi = 0^\circ$ ) was the most energetically stable cluster (with a difference in electronic energy of 0.31 eV in the gas phase and 0.23 eV in aqueous solution). As experimentally observed, two weak and redshifted transitions ( $S_0 \rightarrow S_4$ ,  $f = 0.14$ ,  $\Delta E = -0.14$  eV;  $S_0 \rightarrow S_5$ ,  $f = 0.15$ ,  $\Delta E = -0.08$  eV) were calculated for  $t_1$  in aqueous solution (see Table S6 in the Supporting Information for more details). Other remarkable results extracted from DFT calculations include the strong electronic coupling found in cluster  $t_1$  of **3** ( $|t_h t_e| \approx 0.85$  eV; see Table 2). As previously discussed, the loss of planarity of **3** in the excited state seems to be one of the causes of the low fluorescence quantum yield of this molecule, but the formation of a strongly coupled aggregate could reduce the deformation of the molecular structure in the  $S_1$  state, and thus, increase its fluorescence. Accordingly, the highest fluorescence anisotropy values were also found for compound **3**, which suggested that the movement of this molecule was more restricted in the aggregate than that in aggregates formed for **1** and **2** under similar experimental conditions (see Table 3). Time-resolved fluorescence experiments showed the coexistence of different emissive species in aggregates formed at  $f_w \geq 30\%$  due to significant differences in the value of  $\tau_{av}$  at different wavelengths (see Table 3).

### Solid state

The supramolecular structure was analyzed by means of TEM analysis of solid samples obtained by evaporation of dilute solutions in acetonitrile. We already reported that compound **1** gave rise to nanometer-scale ordered structures inside larger amorphous aggregates and fibers, showing lattice fringes with a periodicity of approximately 0.88–0.92 nm.<sup>[43]</sup> Discotic conjugated molecules tend to form columnar mesophases through  $\pi$ - $\pi$  stacking interactions and these lattice fringes, with a periodicity of tenths of nanometers, are generally associated with the intracolumnar periodicity.<sup>[2,5]</sup> On the other hand, larger lattice fringes, with periodicities of several nanometers, are assigned to the intercolumnar distance (for instance, 2.48 nm in the case of hexa-*peri*-hexabenzocoronene).<sup>[68]</sup> TEM images of solid samples of compounds **2** and **3** are shown in Figure 8 (see also Table S2 in the Supporting Information). For compound **2**, dendritic structures on the submicron scale, exhibiting a nanodomain texture with a high degree of internal order and  $d$  spacings of 0.21 nm, were observed. On the other hand, the structures observed for compound **3** are more similar to those reported for **1**, that is, lattice fringes with a periodicity of 0.70 nm inside larger amorphous fiber-shaped aggregates. Consequently, the cross-shaped core of compound **2** favors the formation of ordered structures with narrower lattice fringes than that in the case of star-shaped molecules. A similar observation was made for the derivatives of **1** and **2** with  $-\text{CH}_2-\text{NH}-(\text{CH}_2)_2-\text{NH}_2$  side chains instead of  $-\text{CH}_2-(\text{CH}_2)_5-\text{OH}$ , that is, the lattice-fringe periodicity decreases from 0.34 to 0.20 nm for derivatives of **1** and **2**, respectively.<sup>[69,70]</sup> Accordingly, the larger conjugated core of **2** seems to favor  $\pi$ -stacking interactions, approximating molecules in the supramolecular structure, with dramatic effects on the luminescence emission properties be-

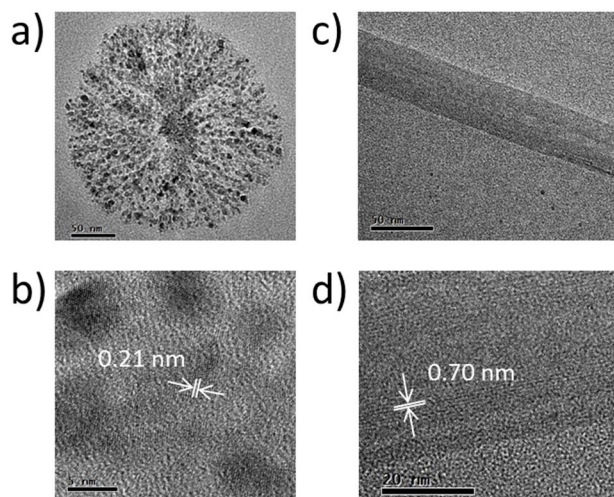


**Figure 8.** TEM images of solid samples of compounds **2** (a,b) and **3** (c,d) obtained by evaporation of dilute solutions in acetonitrile.

cause  $\Phi_F$  drops by up to 1.7% in the solid state (see Figure S10 and Table S2 in the Supporting Information). On the contrary, a high quantum yield of 50.0%<sup>[43]</sup> was reported for compound **1**; this value is associated with X aggregation, which is the most effective molecular arrangement for preventing quenching in the solid state.<sup>[61,71–74]</sup> In the case of compound **3**, a weak solid-state luminescence enhancement (SLE) effect was found because  $\Phi_F$  increased from values of  $\leq 1.3\%$  in solution to 5.5% in the solid state. In the solid state, this phenomenon could be explained through the same mechanism of AIEE observed for molecular aggregates in solvent mixtures with high water fractions, that is, molecule **3** is highly planar in the  $S_0$  state and tends to establish strong supramolecular interactions that could constrain the molecule and reduce its deformation in the  $S_1$  state, and thus, increase the luminescence of the solid. As a consequence, for the set of compounds studied, the star-shaped styrylbenzene derivatives seem to be the best choice for solid light-emitting applications without considering their semiconducting performance.

## Conclusion

We have analyzed the photophysical properties of a set of star- and cross-shaped conjugated molecules in three states: free molecules, molecular aggregates in solution, and the solid state. AIEE and SLE phenomena were observed for some of these molecules under certain experimental conditions. Different spectroscopic experiments and DFT calculations were conducted to unravel the mechanisms responsible for the observed fluorescence enhancement.

AIEE was found for compound **1** in mixtures of water/acetonitrile and water/tetrahydrofuran with low water fractions. This fact was associated with the RIV mechanism (restriction of wide wagging modes of the molecule) and the blocking of  $E/Z$  photoisomerization in the  $\pi$ -stacking aggregates. On the contrary, RIV seems to be a less efficient mechanism for compound **2** because several normal modes, with significant HR

factor values, correspond to slight rocking of the phenyl rings that cannot be totally blocked in the  $\pi$ -stacking aggregate, and thus, contributes to nonradiative deactivation. In addition, it was predicted that  $E/Z$  photoisomerization was a less efficient nonradiative mechanism for compound **2** than that for **1**, on the basis of the significant energy difference calculated for  $E/Z$ -rotation barriers of both compounds in the  $S_1$  state. Consequently, AIEE is not observed for compound **2** in contrast to that of **1**. Compound **3** showed AIEE in mixtures of water/acetonitrile with high water fractions. Although this molecule is highly planar in the  $S_0$  state, it was theoretically predicted to lose planarity upon electronic excitation. The formation of strongly coupled aggregates could constrain the molecule and reduce its deformation in the  $S_1$  state, and thus, increase its luminescence in solution (AIEE). The SLE phenomenon, also observed for **3**, can be explained through a similar mechanism involving strong supramolecular interactions that constrain the molecule in the solid state.

## Experimental Section

### Synthesis

The formation of the double bonds in compounds **1**<sup>[43]</sup> and **2** was performed by the HWE reaction of 4-hexyloxybenzaldehyde and the corresponding benzyl phosphonate by following a standard methodology. Compound **3** was isolated from 4-hexyloxybenzaldehyde after its reaction with trimethyl-*s*-triazine in the presence of a base. Details concerning the synthesis and chemical characterization of compounds **2** and **3** are provided in the Supporting Information.

### Spectroscopy and microscopy: Experimental details

The general experimental conditions for spectroscopy and microscopy measurements are provided in the Supporting Information. The specific conditions of each experiment are indicated in the tables and figure captions.

### Computational details and theoretical background

Full geometry optimizations were performed by using the Gaussian 09 (Revision D.01) suite of programs<sup>[75]</sup> at the M06-2X/6-31G\* level of theory.<sup>[76]</sup> We chose the metahybrid M06-2X functional due to its satisfactory performance in the calculation of optoelectronic properties and noncovalent interactions of related compounds.<sup>[43,47,48]</sup> The molecular geometries of the ground state,  $S_0$ , and the first excited state,  $S_1$ , were optimized and the vibrational modes were calculated to check the absence of imaginary frequencies. The solvent environment was described by the polarizable continuum model (PCM), as implemented in the Gaussian package.<sup>[77–79]</sup> The reorganization energy,  $\lambda$ , associated with electronic relaxation was calculated by using the DUSHIN program,<sup>[80]</sup> according to Equation (1):

$$\lambda = \sum_i \lambda_i = \sum_i \hbar \omega_i S_i \quad (1)$$

in which  $\omega_i$  is the wavenumber associated to the vibrational mode  $i$ , and  $S_i$  is the HR parameter calculated from the atomic displacements  $\Delta Q$  and force constant,  $k$ , of the normal mode  $i$ , according to Equation (2):

$$S_i = \frac{1}{2} k \frac{\Delta Q^2}{h\omega_i} \quad (2)$$

Values of  $\lambda$  and HR factors allow us to identify the vibrational modes involved in nonradiative, internal conversion decay.<sup>[81]</sup>

To shed light on the changes found in the photophysical properties of the studied molecules upon aggregation, diverse model clusters made of four monomers were optimized by using the ONIOM methodology<sup>[82–84]</sup> in both the gas phase and aqueous solution. The high layer ( $\pi$ -conjugated central cores) was optimized at the M06-2X/6-31G\* level of theory, whereas M06-2X/STO-3G was used for the lower accuracy layer (alkoxy side chains). The dispersion interactions in the cluster optimizations were considered with the Grimme D3 dispersion correction,<sup>[85]</sup> with the original D3 damping function, as implemented in Gaussian 09.<sup>[75]</sup> The starting points for the molecular cluster optimizations were constructed in three steps: 1) a rotational barrier around the azimuthal angle ( $\varphi$ ) of a fully overlapped dimer was analyzed for the compounds studied (see Figure 9); 2) the binding energy was calculated as a function of the relative  $x$  and  $y$  displacement for  $\varphi = 0$  (fully overlapped

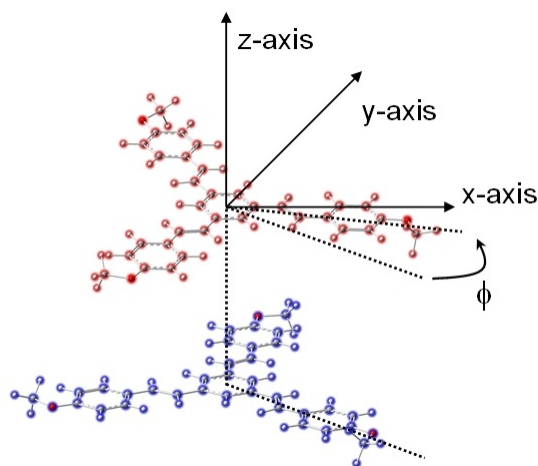


**Figure 9.** Representation of the two stacked molecules used for the binding-energy landscapes showing the azimuthal angle ( $\varphi$ ) and the  $x$  and  $y$  displacement directions.

configuration) and  $\varphi$  values associated with energy minima found in the azimuthal barrier (the interdisk distance was fixed at 5.1 and 3.5 Å for compounds **2** and **3**, respectively); and 3) the tetramer cluster was constructed by employing the molecular arrangement of the maximum binding energy obtained in the previous step as a starting point (see Figure S18 in the Supporting Information). In the context of the framework reported by Spano and Heestand,<sup>[35,36]</sup> the photophysical signatures in the aggregates are the result of competition between long-range Coulomb interactions (Kasha model) and short-range charge-transfer interactions. The latter could induce photophysical behavior of J/H aggregates because the charge-transfer intermolecular coupling,  $J_{CT}$  was proportional to  $-|t_e t_h|$ , in which  $t_e$  and  $t_h$  represented the electron and hole couplings, respectively, calculated at the M06-2X/6-31G\* level of theory by using the splitting method,<sup>[86]</sup> according to Equations (3) and (4):

$$t_h = \frac{E_{\text{HOMO}} - E_{\text{HOMO}-1}}{2} \quad (3)$$

$$t_e = \frac{E_{\text{LUMO}+1} - E_{\text{LUMO}}}{2} \quad (4)$$

in which  $E_{\text{HOMO(LUMO)}}$  and  $E_{\text{HOMO}-1(\text{LUMO}+1)}$  are the energies of HOMO-(LUMO) and HOMO-1(LUMO+1) energy levels, respectively, taken from the closed-shell configuration of the neutral state of stacked dimers. These dimer clusters were extracted from the central part of the previously optimized molecular tetramers (see Figure S19 in the Supporting Information).

Time-dependent DFT calculations were performed to compute the absorption and emission electronic transitions over the optimized free molecules in the gas phase and in solution. To check the effect of molecular stacking on electronic transitions, the vertical electronic transitions were also computed over molecular di- and tetramers. Tetramer clusters were previously optimized, as described before, and dimer clusters were extracted from the central part of the tetramers (see Figure S19 in the Supporting Information).

## Acknowledgements

We would like to thank the Ministerio de Economía y Competitividad (Spain; project CTQ2017-84561-P) for supporting the research described in this article and the Universidad de Castilla-La Mancha for additional support of the research group (grants GI20163441, 2019-GRIN-27152, and GI20173955). R.D. thanks the Junta de Comunidades de Castilla-La Mancha, Fondo Social Europeo (FSE), and Iniciativa de Empleo Juvenil (EIJ) for the postdoctoral grant. The computation study was financially supported by Consejería de Economía y Conocimiento, the Junta de Andalucía (FQM-337), and Acción 1\_Plan 2017-18 (Universidad de Jaén, Spain). We also thank the Centro de Servicios de Informática y Redes de Comunicaciones (CSIRC; Universidad de Granada, Spain) and the Servicio de Supercomputación de la Universidad de Castilla-La Mancha for providing the computing time.

## Conflict of interest

The authors declare no conflict of interest.

**Keywords:** aggregation · luminescence · photochemistry · self-assembly · styrylbenzenes

- [1] S. I. Stupp, L. C. Palmer, *Chem. Mater.* **2014**, *26*, 507–518.
- [2] E. Busseron, Y. Ruff, E. Moulin, N. Giuseppone, *Nanoscale* **2013**, *5*, 7098–7140.
- [3] Y. Guo, L. Xu, H. Liu, Y. Li, C. M. Che, Y. Li, *Adv. Mater.* **2015**, *27*, 985–1013.
- [4] Y. Yamamoto, *Sci. Technol. Adv. Mater.* **2012**, *13*, 033001–033016.
- [5] F. J. M. Hoeben, P. Jonkheijm, E. W. Meijer, A. P. H. J. Schenning, *Chem. Rev.* **2005**, *105*, 1491–1546.
- [6] T. Wöhrle, I. Wurzbach, J. Kirres, A. Kostidou, N. Kapernaum, J. Litterscheidt, J. C. Haenl, P. Staffeld, A. Baro, F. Giesselmann, S. Laschat, *Chem. Rev.* **2016**, *116*, 1139–1241.
- [7] T. Wu, J. Huang, Y. Yan, *Chem. Asian J.* **2019**, *14*, 730–750.
- [8] Y. Li, Y. Dong, L. Cheng, C. Qin, H. Nian, H. Zhang, Y. Yu, L. Cao, *J. Am. Chem. Soc.* **2019**, *141*, 8412–8415.
- [9] M. J. M. Wells, H. A. Stretz, *Sci. Total Environ.* **2019**, *671*, 1125–1133.
- [10] B. Li, T. He, X. Shen, D. Tang, S. Yin, *Polym. Chem.* **2019**, *10*, 796–818.

- [11] T. Vehoff, Y. S. Chung, K. Johnston, A. Troisi, D. Y. Yoon, D. Andrienko, *J. Phys. Chem. C* **2010**, *114*, 10592–10597.
- [12] L. Jin, H. Wang, Y. Yang, *J. Colloid Interface Sci.* **2013**, *393*, 53–57.
- [13] P. A. Korevaar, T. F. A. de Greef, E. W. Meijer, *Chem. Mater.* **2014**, *26*, 576–586.
- [14] H. Wang, E. Zhao, J. W. Y. Lam, B. Z. Tang, *Mater. Today* **2015**, *18*, 365–377.
- [15] S. Chen, P. Slattum, C. Wang, L. Zang, *Chem. Rev.* **2015**, *115*, 11967–11998.
- [16] P. J. Pacheco-Liñán, M. Moral, M. L. Nueda, R. Cruz-Sánchez, J. Fernández-Sainz, A. Garzón-Ruiz, I. Bravo, M. Melguizo, J. Laborda, J. Albaladejo, *J. Phys. Chem. C* **2017**, *121*, 24786–24797.
- [17] D. Xu, H. Zou, M. Liu, J. Tian, H. Huang, Q. Wan, Y. Dai, Y. Wen, X. Zhang, Y. Wei, *J. Colloid Interface Sci.* **2017**, *508*, 248–253.
- [18] T. Xue, X. Jia, J. Wang, J. Xiang, W. Wang, J. Du, Y. He, *Chem. Eur. J.* **2019**, *25*, 9634–9638.
- [19] T. Xue, J. Shen, K. Shao, W. Wang, B. Wu, Y. He, *Chem. Eur. J.* **2019**, <https://doi.org/10.1002/chem.201904327>.
- [20] A. C. Rodrigo, I. Rivilla, F. C. Pérez-Martínez, S. Monteagudo, V. Ocaña, J. Guerra, J. C. García-Martínez, S. Merino, P. Sánchez-Verdu, V. Ceña, J. Rodríguez-López, *Biomacromolecules* **2011**, *12*, 1205–1213.
- [21] C. C. Cheng, B. T. Gebeyehu, S. Y. Huang, Y. A. Alemayehu, Y. T. Sun, Y. C. Lai, Y. H. Chang, J. Y. Lai, D. J. Lee, *J. Colloid Interface Sci.* **2019**, *552*, 166–178.
- [22] W. T. Koo, J. S. Jang, I. D. Kim, *Chem.* **2019**, *5*, 1938–1963.
- [23] Y. Qi, Y. Wang, Y. Yu, Z. Liu, Y. Zhang, Y. Qi, C. Zhou, *J. Mater. Chem. C* **2016**, *4*, 11291–11297.
- [24] J. R. Lakowicz, *Principles of Fluorescence Spectroscopy*, 3rd ed., Springer, New York, **2006**.
- [25] J. Mei, N. L. C. Leung, R. T. K. Kwok, J. W. Y. Lam, B. Z. Tang, *Chem. Rev.* **2015**, *115*, 11718–11940.
- [26] Y. Hong, J. W. Y. Lam, B. Z. Tang, *Chem. Soc. Rev.* **2011**, *40*, 5361–5388.
- [27] M. Yamaguchi, S. Ito, A. Hirose, K. Tanaka, Y. Chujo, *Mater. Chem. Front.* **2017**, *1*, 1573–1579.
- [28] J. Yang, J. Huang, Q. Li, Z. Li, *J. Mater. Chem. C* **2016**, *4*, 2663–2684.
- [29] W. Yao, Y. Yan, L. Xue, C. Zhang, G. Li, Q. Zheng, Y. S. Zhao, H. Jiang, J. Yao, *Angew. Chem. Int. Ed.* **2013**, *52*, 8713–8717; *Angew. Chem.* **2013**, *125*, 8875–8879.
- [30] S. Kumar, M. Singh, P. Gaur, J. H. Jou, S. Ghosh, *ACS Omega* **2017**, *2*, 5348–5356.
- [31] C. Niu, Y. You, L. Zhao, D. He, N. Na, J. Ouyang, *Chem. Eur. J.* **2015**, *21*, 13983–13990.
- [32] E. G. McRae, M. Kasha, *J. Chem. Phys.* **1958**, *28*, 721.
- [33] M. Kasha, *Radiat. Res.* **1963**, *20*, 55–71.
- [34] M. Kasha, H. R. Rawls, M. Ashraf El-Bayoumi, *Pure Appl. Chem.* **1965**, *11*, 371–392.
- [35] N. J. Hestand, F. C. Spano, *Acc. Chem. Res.* **2017**, *50*, 341–350.
- [36] N. J. Hestand, F. C. Spano, *Chem. Rev.* **2018**, *118*, 7069–7163.
- [37] R. Crespo-Otero, Q. Li, L. Blancafort, *Chem. Asian J.* **2019**, *14*, 700–714.
- [38] J. Shi, L. E. Aguilar Suarez, S. J. Yoon, S. Varghese, C. Serpa, S. Y. Park, L. Lüer, D. Roca-Sanjuán, B. Milián-Medina, J. Gierschner, *J. Phys. Chem. C* **2017**, *121*, 23166–23183.
- [39] T. Costa, L. E. Garner, M. Knaapila, A. W. Thomas, S. E. Rogers, G. C. Bazan, H. D. Burrows, *Langmuir* **2013**, *29*, 10047–10058.
- [40] S. Mu, K. Oniwa, T. Jin, N. Asao, M. Yamashita, S. Takaishi, *Org. Electron.* **2016**, *34*, 23–27.
- [41] Z. Xu, Q. Liao, Y. Wu, W. Ren, W. Li, L. Liu, S. Wang, Z. Gu, H. Zhang, H. Fu, *J. Mater. Chem.* **2012**, *22*, 17737–17743.
- [42] O. K. Nag, C. S. Lim, B. L. Nguyen, B. Kim, J. Jang, J. H. Han, B. R. Cho, H. Y. Woo, *J. Mater. Chem.* **2012**, *22*, 1977–1984.
- [43] A. Garzón, M. P. Fernández-Lienres, M. Moral, T. Peña-Ruiz, A. Navarro, J. Tolosa, J. Canales-Vázquez, D. Hermida-Merino, I. Bravo, J. Albaladejo, J. C. García-Martínez, *J. Phys. Chem. C* **2017**, *121*, 4720–4733.
- [44] J. C. García-Martínez, E. Díez-Barra, J. Rodríguez-López, *Curr. Org. Synth.* **2008**, *5*, 267–269.
- [45] E. Díez-Barra, J. C. García-Martínez, S. Merino, R. del Rey, J. Rodríguez-López, P. Sánchez-Verdú, J. Tejeda, *J. Org. Chem.* **2001**, *66*, 5664–5670.
- [46] H. C. Holst, T. Pakula, H. Meier, *Tetrahedron* **2004**, *60*, 6765–6775.
- [47] M. Moral, R. Domínguez, M. P. Fernández-Lienres, A. Garzón-Ruiz, J. C. García-Martínez, A. Navarro, *J. Chem. Phys.* **2019**, *150*, 064309.
- [48] M. Moral, J. Tolosa, J. Canales-Vázquez, J. C. Sancho-García, A. Garzón-Ruiz, J. C. García-Martínez, *J. Phys. Chem. C* **2019**, *123*, 11179–11188.
- [49] I. N. Levine, *Physical Chemistry*, 6th ed., McGraw Hill, New York, **2009**.
- [50] S. J. Strickler, R. A. Berg, *J. Chem. Phys.* **1962**, *37*, 814–821.
- [51] J. P. Vikesland, S. J. Strickler, *J. Chem. Phys.* **1974**, *60*, 660–663.
- [52] M. Fecková, P. le Poul, F. Robin-le Guen, T. Roisnel, O. Pytela, M. Klikar, F. Bures, S. Achelle, *J. Org. Chem.* **2018**, *83*, 11712–11726.
- [53] P. Ehlers, A. Hakobyan, A. Neubauer, S. Lochbrunner, P. Langer, *Adv. Synth. Catal.* **2013**, *355*, 1849–1858.
- [54] H. Hassanain, E. S. Davies, W. Lewis, D. L. Kays, N. R. Champness, *CrystrEngComm* **2019**, *21*, 4551–4556.
- [55] S. H. Hsiao, H. M. Wang, S. H. Liao, *Polym. Chem.* **2014**, *5*, 2473–2483.
- [56] Y. Wang, S. Mori, H. Furuta, S. Shimizu, *Angew. Chem. Int. Ed.* **2019**, *58*, 10975–10979; *Angew. Chem.* **2019**, *131*, 11091–11095.
- [57] G. de Miguel, L. Camacho, E. M. García-Frutos, *J. Mater. Chem. C* **2016**, *4*, 1208–1214.
- [58] D. Oelkrug, K. Rempfer, E. Prass, H. Meier, *Zeitschrift für Naturforschung A* **1988**, *43*, 583–590.
- [59] H. Meier, R. Zertani, K. Noller, D. Oelkrug, G. Krabichler, *Chem. Ber.* **1986**, *119*, 1716–1724.
- [60] Y. Qian, M. Cai, X. Zhou, Z. Gao, X. Wang, Y. Zhao, X. Yan, W. Wei, L. Xie, W. Huang, *J. Phys. Chem. C* **2012**, *116*, 12187–12195.
- [61] Y. J. Wang, Z. Li, J. Tong, X. Y. Shen, A. Qin, J. Z. Sun, B. Z. Tang, *J. Mater. Chem. C* **2015**, *3*, 3559–3568.
- [62] X. Zhang, J. Ye, L. Xu, L. Yang, D. Deng, G. Ning, *J. Lumin.* **2013**, *139*, 28–34.
- [63] J. Ye, Y. Gao, L. He, T. Tan, W. Chen, Y. Liu, Y. Wang, C. Ning, *Dyes Pigm.* **2016**, *124*, 145–155.
- [64] S. Ge, B. Li, X. Meng, H. Yan, M. Yang, B. Dong, Y. Lu, *Dyes Pigm.* **2018**, *148*, 147–153.
- [65] M. Klessinger, J. Michl, *Excited States and Photochemistry of Organic Molecules*, Wiley-VCH, Weinheim, **1995**.
- [66] L. Le Bras, K. Chaitou, S. Aloïse, C. Adamo, A. Perrier, *Phys. Chem. Chem. Phys.* **2019**, *21*, 46–56.
- [67] I. N. Ioffe, A. A. Granovsky, *J. Chem. Theory Comput.* **2013**, *9*, 4973–4990.
- [68] W. Pisula, A. Menon, M. Stepputat, I. Lieberwirth, U. Kolb, A. Tracz, H. Siringhaus, T. Pakula, K. Müllen, *Adv. Mater.* **2005**, *17*, 684–689.
- [69] P. J. Pacheco-Liñán, A. Garzón, J. Tolosa, I. Bravo, J. Canales-Vázquez, J. Rodríguez-López, J. Albaladejo, J. C. García-Martínez, *J. Phys. Chem. C* **2016**, *120*, 18771–18779.
- [70] R. Domínguez, J. Tolosa, M. Moral, I. Bravo, J. Canales-Vázquez, J. Rodríguez-López, A. Garzón-Ruiz, J. C. García-Martínez, *J. Phys. Chem. C* **2018**, *122*, 19937–19945.
- [71] J. Zhang, B. Xu, J. Chen, S. Ma, Y. Dong, L. Wang, B. Li, L. Ye, W. Tian, *Adv. Mater.* **2014**, *26*, 739–745.
- [72] X. Feng, J. Y. Hu, F. Iwanaga, N. Seto, C. Redshaw, M. R. J. Elsegood, T. Yamato, *Org. Lett.* **2013**, *15*, 1318–1321.
- [73] Z. Xie, B. Yang, F. Li, G. Cheng, L. Liu, G. Yang, H. Xu, L. Ye, M. Hanif, S. Liu, D. Ma, Y. Ma, *J. Am. Chem. Soc.* **2005**, *127*, 14152–14153.
- [74] J. Liu, L. Meng, W. Zhu, C. Zhang, H. Zhang, Y. Yao, Z. Wang, P. He, X. Zhang, Y. Wang, Y. Zhen, H. Dong, Y. Yia, W. Hu, *J. Mater. Chem. C* **2015**, *3*, 3068–3071.
- [75] Gaussian 09 (Revision D.01), M. J. Frisch, G. W. Trucks, H. B. Schlegel, G. E. Scuseria, M. A. Robb, J. R. Cheeseman, G. Scalmani, V. Barone, G. A. Petersson, H. Nakatsuji, X. Li, M. Caricato, A. Marenich, J. Bloino, B. G. Janesko, R. Gomperts, B. Mennucci, H. P. Hratchian, J. V. Ortiz, A. F. Izmaylov, J. L. Sonnenberg, D. Williams-Young, F. Ding, F. Lipparini, F. Egidi, J. Goings, B. Peng, A. Petrone, T. Henderson, D. Ranasinghe, V. G. Zakrzewski, J. Gao, N. Rega, G. Zheng, W. Liang, M. Hada, M. Ehara, K. Toyota, R. Fukuda, J. Hasegawa, M. Ishida, T. Nakajima, Y. Honda, O. Kitao, H. Nakai, T. Vreven, K. Throssell, J. A. Montgomery, Jr., J. E. Peralta, F. Ogliaro, M. Bearpark, J. J. Heyd, E. Brothers, K. N. Kudin, V. N. Staroverov, T. Keith, R. Kobayashi, J. Normand, K. Raghavachari, A. Rendell, J. C. Burant, S. S. Iyengar, J. Tomasi, M. Cossi, J. M. Millam, M. Klene, C. Adamo, R. Cammi, J. W. Ochterski, R. L. Martin, K. Morokuma, O. Farkas, J. B. Foresman, D. J. Fox, Gaussian, Inc., Wallingford CT, **2009**.
- [76] Y. Zhao, D. G. Truhlar, *Theor. Chem. Acc.* **2008**, *120*, 215–241.
- [77] M. Cossi, N. Rega, G. Scalmani, V. Barone, *J. Comput. Chem.* **2003**, *24*, 669–681.
- [78] J. Tomasi, B. Mennucci, R. Cammi, *Chem. Rev.* **2005**, *105*, 2999–3094.

- [79] R. Cammi, S. Corni, B. Mennucci, J. Tomasi, *J. Chem. Phys.* **2005**, *122*, 104513.
- [80] J. R. Reimers, *J. Chem. Phys.* **2001**, *115*, 9103.
- [81] A. Köhler, H. Bässler, *Electronic Processes in Organic Semiconductors: An Introduction*, Wiley-VCH, Weinheim, **2015**.
- [82] S. Dapprich, I. Komaromi, K. S. Byun, K. Morokuma, M. J. Frisch, *J. Mol. Struct.* **1999**, *461–462*, 1–21.
- [83] T. Vreven, K. Morokuma, O. Farkas, H. B. Schlegel, M. J. Frisch, *J. Comput. Chem.* **2003**, *24*, 760–769.
- [84] H. Lin, D. Truhlar, *Theor. Chem. Acc.* **2007**, *117*, 185–199.
- [85] S. Grimme, J. Antony, S. Ehrlich, H. Krieg, *J. Chem. Phys.* **2010**, *132*, 154104.
- [86] V. Coropceanu, J. Cornil, D. A. da Silva Filho, Y. Olivier, R. Silbey, J. L. Brédas, *Chem. Rev.* **2007**, *107*, 926–952.

---

Manuscript received: November 25, 2019  
Revised manuscript received: January 10, 2020  
Version of record online: February 19, 2020